IEEE Access
Multidisciplinary | Rapid Review | Open Access Journal

Received 26 September 2023, accepted 14 October 2023, date of publication 18 October 2023, date of current version 26 October 2023.

Digital Object Identifier 10.1109/ACCESS.2023.3325395

RESEARCH ARTICLE

Characteristics Evaluation of 14 Battery Equivalent Circuit Models

SUNGHUN JUNG[1], (Member, IEEE), AND ABERA TULLU[2], (Member, IEEE)
[1]Faculty of Smart Vehicle System Engineering, Chosun University, Dong-gu, Gwangju 61452, South Korea
[2]Department of Smart Air Mobility, Korea Aerospace University, Deogyang-gu, Goyang 10540, South Korea

Corresponding author: Abera Tullu (tuaberash@gmail.com)

This work was supported by the Research Fund from Chosun University, in 2020, under Grant K208419001.

ABSTRACT In this study, we formulate and implement 14 widely used battery-equivalent circuit models (ECMs) in a MATLAB/Simulink environment and extract the parameters using the hybrid pulse power characterization (HPPC) test results based on the parameter estimator app working on the curve-fitting method. Using the extracted parameter values, which are either state of charge-dependent sixth-degree polynomials or constants, we perform an error fluctuation deviation analysis on two different real flight test results by loading 0 kg and 10 kg payloads on a hexacopter unmanned aerial vehicle for the ECM characteristic evaluation. According to the error characteristic analysis, the Liu ECM resulted in the lowest root mean square (RMS) (0.0376 V), standard deviation (SD) (0.0343 V), and maximum errors (0.6159 V) for the HPPC test, the Rint ECM resulted in the lowest RMS (0.0702 V) and maximum errors (0.6844 V) for the real flight test carrying a 0 kg payload, and the Shepherd ECM resulted in the lowest RMS (0.0875 V) and SD errors (0.0872 V) for the real flight test carrying a 10 kg payload. In conclusion, we recommend the Shepherd ECM with constant parameters owing to its fast parameter optimization convergence time and flexibility to the dynamic discharging load with a smaller error.

INDEX TERMS Battery management systems, equivalent circuit model, unmanned aerial vehicle.

ACRONYMS

BMS	Battery Management System.
CCV	Closed-Circuit Voltage.
DP	Dual Polarization.
ECM	Equivalent Circuit Model.
EV	Electric Vehicle.
GNL	General NonLinear.
HPPC	Hybrid Pulse Power Characterization.
KF	Kalman Filter.
OCV	Open-Circuit Voltage.
PCM	Protection Circuit Module.
PNGV	Partnership for a New Generation of Vehicle.
RC	Resistance-Capacitance.
SD	Standard Deviation.
SOC	State of Charge.
SOH	State of Health.
SOP	State of Power.

The associate editor coordinating the review of this manuscript and approving it for publication was Ilaria De Munari.

I. INTRODUCTION

A. BACKGROUND

Unmanned aerial vehicles (UAV) have become mainstream in civilian markets. Technologies comprising UAV are similar to electric vehicle (EV) technologies in that both systems receive commands from a ground-based pilot/driver, acquire electricity from Li-ion batteries, drive electric motors, and eventually operate wheels/propellers. EVs have evolved from gas-turbine engines and hybrid engine-based UAVs, similar to the EVs that have evolved from internal combustion engine vehicles, hybrid electric vehicles, and plug-in hybrid electric vehicles [1]. Electric UAVs stand out owing to their increased wariness in terms of fuel costs, environmental pollution, and noise problems [2], [3], [4], [5], [6].

Both UAVs and EVs consist of the main subsystems, including the controller, inverter, motor, and battery pack, which are simplified systems compared to traditional internal combustion engine-powered vehicles. This simplified system resulted in fewer malfunctions than before; however, the dependency of both UAVs and EVs on the subsystems

increased simultaneously. Therefore, the accurate monitoring of each subsystem is vital.

A battery management system (BMS) is an electronic system necessary for managing battery packs in normal conditions by collecting cell current, voltage, and temperature data. However, most remotely controlled UAVs only use a protection circuit module (PCM) for battery packs and collect closed-circuit voltage (CCV) data to estimate the usable energy residuals. Therefore, accurate battery state estimation cannot be guaranteed because the system voltage changes dynamically depending on the requested current load owing to the IR-drop phenomenon. A PCM-based battery pack has minimal battery protection functions, including overcharging, over discharging, overcurrent in/out, short circuiting, over/under temperature, and additional functions, including cell balancing and sleep mode operation.

To overcome the limitations of PCMs, researchers have begun applying special state-estimation algorithms. Most advanced battery state estimation algorithms, including the complementary filter, extended Kalman filter (KF), unscented KF, and particle filter, use current, voltage, and temperature data to estimate the battery state of charge (SOC), state of health (SOH), and state of power (SOP), and have been implemented in the BMS [7], [8], [9], [10], [11], [12]. The accurate monitoring of the states of UAVs is much more significant than that of EVs because the inaccurate battery state estimation of the UAV mid-flight may result in the destruction of the entire system.

There are increasing reports of UAV accidents owing to the various risks associated with batteries used in both UAVs and ground control stations [13]. To prevent mishaps in advance, the characteristics of the different types of batteries should be fully understood, appropriate protection hardware and software should be embedded, and periodic maintenance should be performed. A high proportion of the increased number of UAV accidents is related to the absence of a BMS or a minimally functioning PCM; therefore, researchers are looking for solutions by implementing additional concepts, including battery discharge prediction and remaining useful life, which complexifies battery pack-related systems [14], [15].

A BMS manages the cells in a module to monitor their conditions and prevent potential failure. In EVs, several hundred cells are typically used to drive vehicles weighing thousands of kilograms; therefore, modular types containing BMSs would be some of the many applicable choices for effective battery pack replacement or extra maintenance. However, in small- and medium-sized electric vertical takeoff and landing UAVs, which is the focus of this study, only dozens of cells are used; therefore, the centralized type of BMS would be sufficient. Although the centralized BMS is simple, it is still necessary to estimate the exact SOC, SOH, and SOP for the UAV as accurately as for the EV. The typical estimation accuracy ranges of the SOC, SOH, and SOP for EV are approximately 5%, 5%, and 10%, respectively; similar battery state estimation accuracies are necessary for UAV as well [16], [17], [18].

All the above-mentioned state estimation algorithms are built on the battery equivalent circuit model (ECM), which is mainly composed of resistors and capacitors, to calculate the open-circuit voltage (OCV). Most state-estimation algorithms calculate the current SOC value, and the newly calculated SOC data are used as feedback to extract the ECM parameters that are inserted into the state-estimation algorithms to recalculate the current SOC value. These state estimation algorithms are robust against environmental noises or initial offsets but are weak to the innate flaws of the ECM. That is, the ECM accuracy determines the overall SOC, SOH, and SOP state-estimation algorithm accuracy; therefore, the selection of the appropriate ECM depending on the mission characteristics must be prioritized.

B. LITERATURE REVIEW

Many studies have reviewed the most commonly used lumped-parameter-based ECMs, as listed below.

1) The Rint ECM is one of the simplest battery models with only one resistance [19], [20], [21].
2) The Thevenin ECM is an extended version of the Rint model that describes the dynamic characteristics of a battery by including an additional RC branch with a polarization resistance and equivalent capacitance [22].
3) The partnership for a new generation of vehicles (PNGV) ECM is a slightly improved version of the Thevenin ECM, which adds one more equivalent capacitance to describe the variant OCV [19], [20].
4) The dual polarization (DP) ECM, which is an improved Thevenin ECM, was achieved by adding an additional RC ladder to the original Thevenin ECM [19], [22].
5) The general nonlinear (GNL) ECM introduces an RC ladder in addition to the PNGV ECM for the bulk OCV polarization capacitance characteristics [23].
6) The improved RC ECM contains two capacitors and three resistors, such as the RC ECM developed by the SAFT Battery Company; however, their locations are slightly different, which is intended to represent the surface effects and the capability to store chemical charges [19], [20], [24].

7-9) The Shepherd [25], [26], Unnewehr Universal [26], and Nernst [26] ECMs are among the most popular classical ECMs that have been used as foundations for various extended ECM versions, particularly the Plett ECM, which is a combination of all three classic ECMs.

10) To account for the drastically varying battery behaviors, the Fang ECM uses two additional time constants compared with the Nernst ECM [27].
11) To account for fast-current dynamics, the Liu ECM uses a parameter, I_L^*, representing the low-pass-filtered current [28].

12-13) The Tremblay1 ECM [29] and Tremblay2 ECM [30], [31] use similar parameters to those used in

FIGURE 1. Exterior appearance of the Tattu battery pack.

TABLE 1. Specifications of the Tattu battery pack.

Manufacturer	Tattu
Type	Li-Po 6S1P
Voltage (V)	22.2
Capacity (Ah)	22
Size (mm^3)	198×91×66
Weight (kg)	2.40
Continuous C-rate (C)	18
Maximum C-rate (C)	50

Liu ECM but have a considerably simpler approach for calculating those parameters, requiring only three data point sets: (U_{full}, Q_{max}), (U_{exp}, Q_{exp}), and (U_{norm}, Q_{norm}), from the discharge curve.

14) The Plett ECM is a mixed model of the Shepherd model, the Unnewehr universal model, and the Nernst model, and performs better than any of these [9], [10], [32].

C. CONTRIBUTION

In this manuscript, in comparison to most review articles [33] which just express narratively the unique methodical characteristics of other articles, we discuss the specificity of 14 ECMs by presenting a schematic diagram and the corresponding equations. We applied real flight current patterns to evaluate the characteristics of 14 ECMs based on fluctuation deviation analysis with the parameters extracted using hybrid pulse power characterization (HPPC) test results based on the curve-fitting method. We focused on evaluating the ECM in terms of accuracy (mean, root mean square (RMS), standard deviation (SD), and maximum values).

D. ARTICLE ORGANIZATION

The remainder of this paper is organized as follows. Sections II and III present the model preparation, experimental preparation, results, and analysis. Finally, the conclusions and future work are explained in Section IV.

II. MODEL PREPARATION

A. BATTERY PACK

A fresh battery pack (Fig. 1 and Table 1) was prepared for the HPPC (dis)charging tests.

B. ECM

A total of 14 battery ECMs are prepared as presented in Table 2.

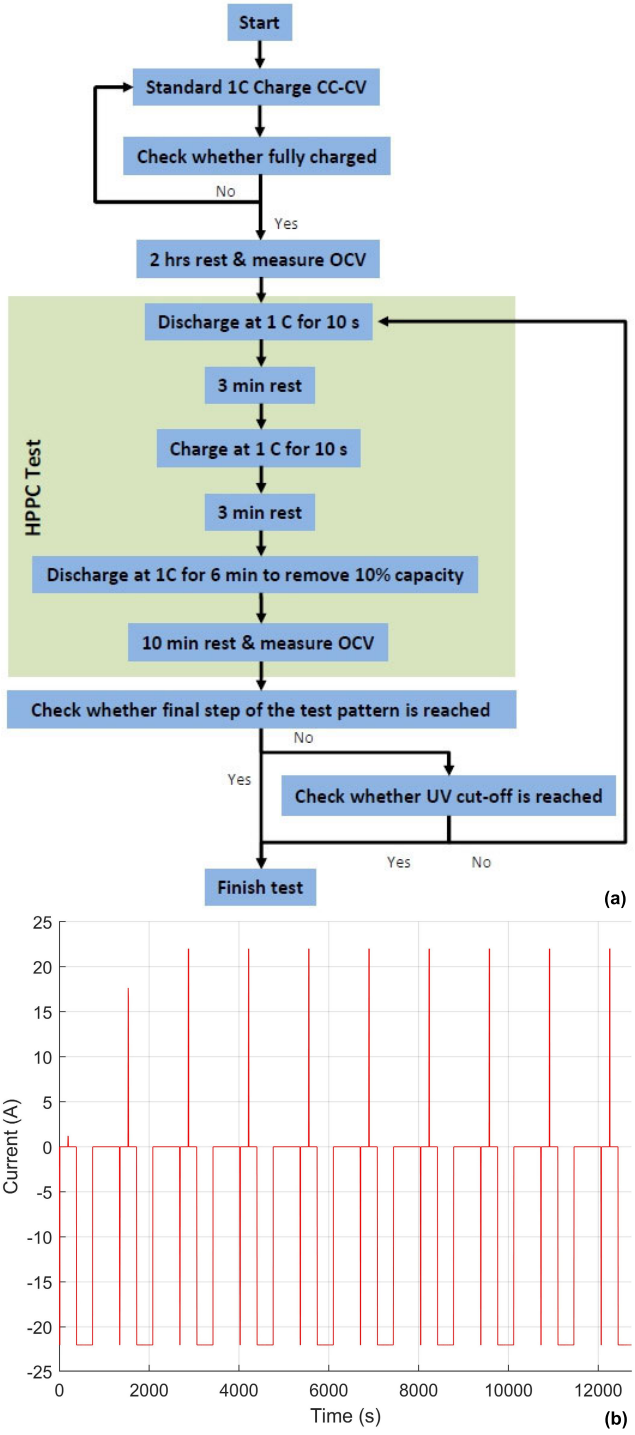

FIGURE 2. HPPC test: (a) schedule, (b) current profile.

C. PARAMETER

1) HPPC TEST

The OCV data acquisition process, that is, the HPPC test, was necessary to derive the ECM parameters. Under a constant environmental temperature of 25 °C, a 1 C-rate of the HPPC current pattern is applied using the direct current (DC) electronic load and DC power supply to retrieve both the dynamic response voltage data and the OCV data per level of SOCs from 100% to 0% with a 10% gap (Fig. 2).

TABLE 2. List of ECMs (dis/charge equations are the same if not divided).

ECM Type		Schematic Diagram	Equation
First Order	(1) Rint [19-21]	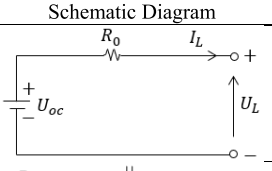	$U_L = U_{oc} - I_L R_0$ (1) where U_L is the CCV (V), U_{oc} is the OCV (V), I_L is the load current (A), and R_0 is the ohmic resistance (Ω)
	(2) Thevenin [22]	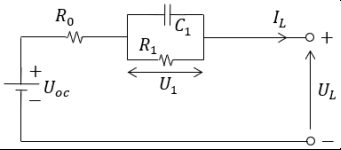	$\dot{U}_1 = -\frac{U_1}{R_1 C_1} + \frac{I_L}{C_1}$ (2) $U_L = U_{oc} - U_1 - I_L R_0$ (3) where U_1 is the voltage on C_1 (V), R_1 is the electrochemical polarization resistance (Ω), and C_1 is the electrochemical polarization capacitance (F)
	(3) PNGV (Improved Thevenin) [19,20]	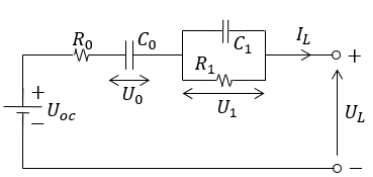	$\dot{U}_0 = \frac{I_L}{C_0}$ (4) $\dot{U}_1 = -\frac{U_1}{R_1 C_1} + \frac{I_L}{C_1}$ (5) $U_L = U_{oc} - U_0 - U_1 - I_L R_0$ (6) where U_0 is the voltage on C_0 (V) and C_0 is the OCV polarization capacitance (F)
Second Order	(4) DP (Improved Thevenin) [19,22]	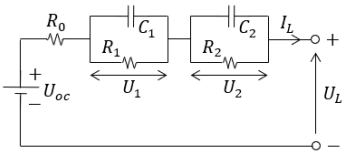	$\dot{U}_1 = -\frac{U_1}{R_1 C_1} + \frac{I_L}{C_1}$ (7) $\dot{U}_2 = -\frac{U_2}{R_2 C_2} + \frac{I_L}{C_2}$ (8) $U_L = U_{oc} - U_1 - U_2 - I_L R_0$ (9) where U_2 is the voltage on C_2 (V), R_2 is the concentration polarization resistance (Ω), and C_2 is the concentration polarization capacitance (F)
	(5) GNL (Improved DP) [23]	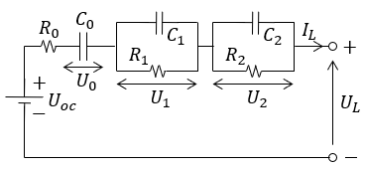	$\dot{U}_0 = \frac{I_L}{C_0}$ (10) $\dot{U}_1 = -\frac{U_1}{R_1 C_1} + \frac{I_L}{C_1}$ (11) $\dot{U}_2 = -\frac{U_2}{R_2 C_2} + \frac{I_L}{C_2}$ (12) $U_L = U_{oc} - U_0 - U_1 - U_2 - I_L R_0$ (13)
(6) Improved RC [19,20,24]		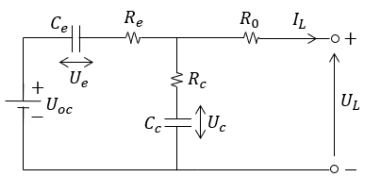	$\dot{U}_e = -\frac{U_e}{C_e(R_e+R_c)} + \frac{U_c}{C_e(R_e+R_c)} - \frac{R_c}{C_e(R_e+R_c)} I_L$ (14) $\dot{U}_c = \frac{U_e}{C_c(R_e+R_c)} - \frac{U_c}{C_c(R_e+R_c)} - \frac{R_e}{C_c(R_e+R_c)} I_L - \frac{I_L}{C_c}$ (15) $U_L = U_{oc} + \frac{R_c}{(R_e+R_c)} U_e + \frac{R_e}{(R_e+R_c)} U_c - \frac{R_e R_c}{(R_e+R_c)} I_L + I_L R_0$ (16) where U_e is the voltage on C_e (V), C_e is the concentration polarization capacitance (F), R_e is the end resistance (Ω), R_c is the capacitor resistance (Ω), and C_c is the surface effect capacitance (F)
(7) Shepherd [25,26]		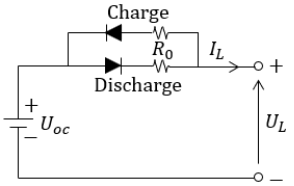	$\dot{z} = -\frac{I_L}{3600Q}$ (17) $U_L = U_{oc} - \frac{K}{z} - I_L R_0$ (18) where Q is the maximum capacity (Ah), K is the polarization resistance (Ω), and z is the SOC $(\%/100)$
(8) Unnewehr Universal [26]			$\dot{z} = -\frac{I_L}{3600Q}$ (19) $U_L = U_{oc} - Kz - I_L R_0$ (20) where K is the polarization resistance (Ω)
(9) Nernst [26]			$\dot{z} = -\frac{I_L}{3600Q}$ (21) $U_L = U_{oc} - K_0 ln(z) + K_1 ln(1-z) - I_L R_0$ (22) where K_i is the constant (V)
(10) Fang (Improved Nernst) [27]			$\dot{z} = -\frac{I_L}{3600Q}$ (23) $U_L = U_{oc} - K_0 ln(\tau_1 + z) + K_1 ln(\tau_2 + 1 - z) - I_L R_0$ (24) where τ_i is the constant (no unit)

TABLE 2. *(Continued.)* List of ECMs (dis/charge equations are the same if not divided).

(11) Liu [28]		$\dot{z} = -\frac{I_L}{3600Q}$ (25) $\dot{I}_L^* = -\frac{I_L^*}{t_c} + \frac{I_L}{t_c}$ (26) Discharge: $U_L = U_{oc} - K\frac{Q(1-z)}{z} - K\frac{I_L^*}{z} + Ae^{-BQ(1-z)} - I_L R_0$ (27) Charge: $U_L = U_{oc} - K\frac{Q(1-z)}{z} - K\frac{I_L^*}{1-z} + Ae^{-BQ(1-z)} - I_L R_0$ (28) where I_L^* is the low pass filtered current (A), t_c is the time constant (s), A is the exponential voltage (V), B is the exponential capacity (Ah^{-1}), and K is the polarization constant (V/Ah) or polarization resistance (Ω)
(12) Tremblay1 [29]		$U_L = U_{oc} - K\frac{Q}{Q - I_L t} + Ae^{-BI_L t} - I_L R_0$ (29)
(13) Tremblay2 [30,31]		$U_{full} = U_{oc} + A - I_L R_0$ (30) $U_{exp} = U_{oc} - K\frac{Q}{Q - Q_{exp}}(Q_{exp} + I_L) + Ae^{\frac{-3}{Q_{exp}}Q_{exp}} - I_L R_0$ (31) $U_{norm} = U_{oc} - K\frac{Q}{Q - Q_{norm}}(Q_{norm} + I_L) + Ae^{\frac{-3}{Q_{exp}}Q_{norm}} - I_L R_0$ (32) Discharge: $U_L = U_{oc} - K\frac{Q}{Q - I_L t}I_L^* - K\frac{Q}{Q - I_L t}I_L t + Ae^{-BI_L t} - I_L R_0$ (33) Charge: $U_L = U_{oc} - K\frac{Q}{I_L t - 0.1Q}I_L^* - K\frac{Q}{Q - I_L t}I_L t + Ae^{-BI_L t} - I_L R_0$ (34) where U_{full} is the fully charged voltage (V), U_{exp} is the voltage at the end of exponential zone (V), U_{norm} is the voltage at the end of nominal zone (V), Q_{exp} is the capacity at the end of exponential zone (Ah), Q_{norm} is the capacity at the end of nominal zone (Ah), t is the step time (s), A is the exponential voltage (V), and B is the exponential capacity (Ah^{-1})
(14) Plett [32- 9]		$\dot{z} = \frac{\eta}{C_n}I_L$ (Discharge: $\eta = 1$, Charge: $\eta \leq 1$) (35) $U_L = K_0 - \frac{K_1}{z} - K_2 z + K_3 ln(z) + K_4 ln(1-z) - I_L R_0$ (36) where η is the battery coulombic efficiency (no unit) and K_i is the constant (V)

a: PARAMETER IDENTIFICATION 1

In the cases of the (1) Rint, (2) Thevenin, (3) PNGV, (4) DP, (5) GNL, and (6) improved RC ECMs in Table 1, the ECM parameters vary depending on the SOC, temperature, and humidity, (dis)charging state, and C-rate. In this study, we focused only on the SOC effect by fitting sixth-degree polynomials (Eq. 37). Curve fitting with higher-order polynomials could result in enhanced approximation, but requires a longer data fitting time, and vice versa.

$$U_{oc} = U_L + I_L R_0 + f\,(R_i, C_i, K_i, A, B) \tag{37}$$

where $R_i = \sum_{k=0}^{6} R_{i,k} z^k$, $C_i = \sum_{k=0}^{6} C_{i,k} z^k$, $K_i = \sum_{k=0}^{6} K_{i,k} z^k$, $A = \sum_{k=0}^{6} A_k z^k$ and $B = \sum_{k=0}^{6} B_k z^k$.

b: PARAMETER IDENTIFICATION 2

In the cases of (7) Shepherd, (8) Unnewehr Universal, (9) Nernst, (10) Fang, (11) Liu, (12) Tremblay1, (13) Tremblay2, and (14) Plett in Table 1, the ECM parameters are independent of the SOC, temperature, humidity, (dis)charging state, and C-rate. Therefore, instead of curve-fitting polynomials, the simulated data were curve-fitted to the measured battery pack CCV, U_L, and data to determine the constant variables resulting in the minimum voltage difference based on the parameter estimator app available in Simulink (Eq. 38).

$$U_{oc} = U_L + I_L R_0 + f\,(K_i, \tau_i, t_c, A, B) \tag{38}$$

where K_i, τ_i, t_c, A and B are all constant parameters.

Here, the measured data are the measured battery pack voltage data from the HPPC test (Fig. 2), whereas the simulated data are the simulated battery pack voltage data generated using one of the listed ECMs (Table 2).

Curve fitting with constant parameters can result in a fast optimization convergence time, but normally loses the flexibility to adapt to new discharge current patterns.

2) OPTIMIZED PARAMETERS

Throughout the parameter identification process described in the previous subsection, the optimum parameter data resulting in the minimum difference between each ECM and the OCV data from the HPPC test were obtained, as illustrated in Table 3, and the corresponding OCV profiles are shown in Fig. 3.

Here, the OCV profile named "Reference" is the OCV data obtained from the HPPC test (Fig. 2).

III. EXPERIMENT

A. PREPARATION

To evaluate the performance of the 14 candidate ECMs, two real-flight current patterns obtained using a hexacopter UAV (Fig. 4) carrying 0 kg and 10 kg payloads were used. It is obvious that the flight time with the 10 kg payloads is much shorter than that with the 0 kg payloads by more than half, owing to the approximately doubled discharge current magnitude.

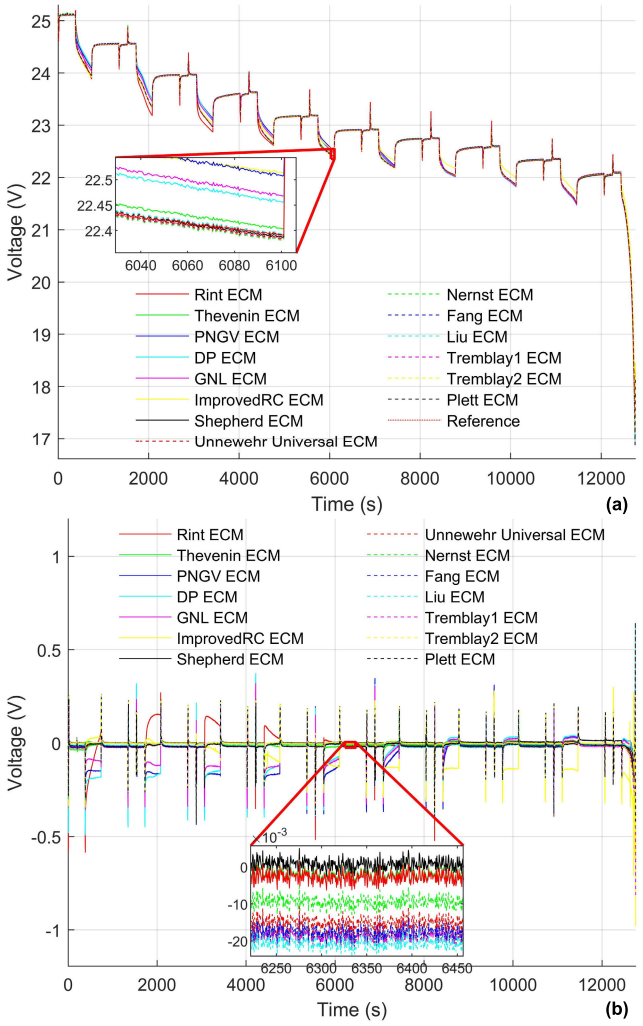

FIGURE 3. Battery pack voltage profiles of U_{oc}: (a) voltage profile, (b) fluctuation deviation.

FIGURE 4. Exterior appearance of Hexacopter UAV.

Real-flight current patterns were applied following the schedule (Fig. 5(a)) using a DC electronic load (Fig. 5(b)). Here, CC-CV represents the constant current-constant voltage, VOC is the open-circuit voltage (V), and UV is the undervoltage limit (V).

Depending on the characteristics of the real flight patterns (either flight or driving patterns) and battery ingredients, the dynamic response of the ECMs might be altered a bit but the general performance characteristics of the individual ECM will be similar even if the application changes since the dynamic response is dependent on variables consisting of the ECM rather than the given load profile.

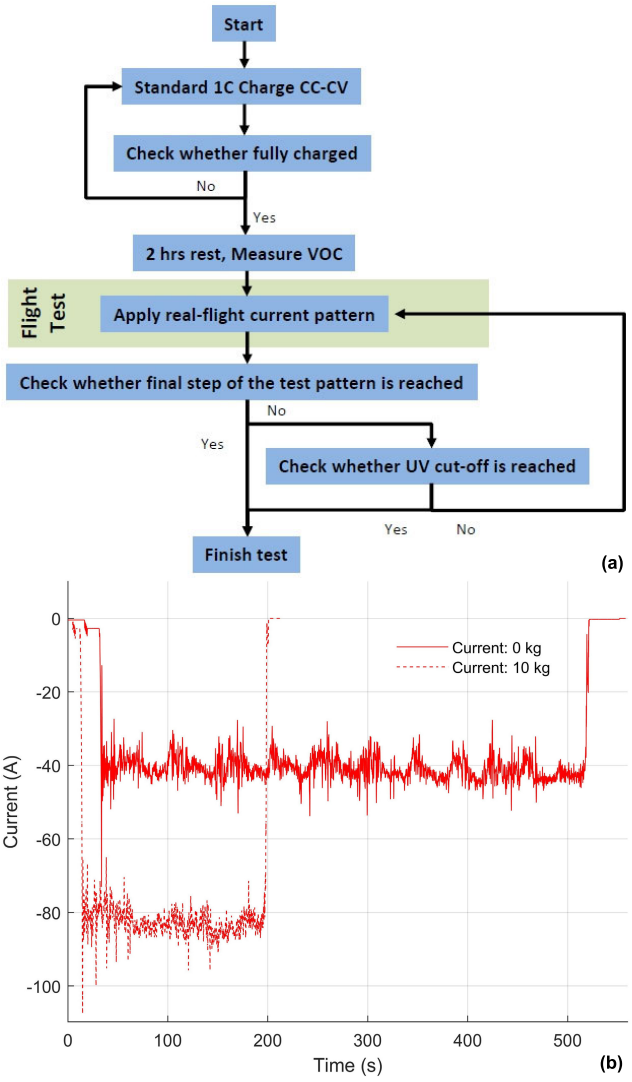

FIGURE 5. Flight test: (a) schedule, (b) current profiles.

B. EXPERIMENTAL RESULT

Figs. 6 and 7 show the CCV and fluctuation deviation profiles corresponding to the flight tests carrying 0 kg and 10 kg payloads. Here, the CCV profile named "Reference" is the CCV data obtained from a real flight test (Fig. 5).

C. ANALYSIS

We summarized the mean, RMS, SD, and maximum errors (Table 4) and observed the following three phenomena.

1) In the case of the HPPC test (orange), that is, U_{oc}, (11), the Liu ECM worked best, resulting in the lowest RMS (0.0376 V), SD (0.0343 V), and maximum errors (0.6159 V).
2) In the case of the real flight test (colored green), that is, U_{cc}, carrying a 0 kg payload, (1) the Rint ECM

TABLE 3. Optimized ECM parameter data.

ECM Type		Para.	Unit	$U_{oc} = U_L + I_L R_0 + f(R_i, C_i, K_i, A, B)$ | $U_{oc} = U_L + I_L R_0 + f(K_i, \tau_i, t_c, A, B)$
First Order	(1) Rint [19-21]	R_0	Ω	$R_0 = 0.4196SOC^6 - 1.1809SOC^5 + 1.2548SOC^4 - 0.6560SOC^3 + 0.1840SOC^2 - 0.0248SOC + 0.0026$
	(2) Thevenin [22]	R_0	Ω	$R_0 = 0.0278SOC^6 - 0.0449SOC^5 + 0.0239SOC^4 - 0.0139SOC^3 + 0.013SOC^2 - 0.0050SOC + 0.002$
		R_1	Ω	$R_1 = -0.0665SOC^6 + 0.24SOC^5 - 0.3426SOC^4 + 0.2525SOC^3 - 0.0879SOC^2 + 0.0088SOC + 0.0059$
		C_1	F	$C_1 = 75085.1921SOC^6 + 119995.6922SOC^5 - 719191.9286SOC^4 + 851068.1861SOC^3 - 392638.096SOC^2 + 58197.0948SOC + 10591.371$
	(3) PNGV (Improved Thevenin) [19,20]	R_0	Ω	$R_0 = 0.0031SOC^6 - 0.0022SOC^5 + 0.0042SOC^4 - 0.0027SOC^3 + 0.0007SOC^2 - 0.0001SOC$
		R_1	Ω	$R_1 = -0.0818SOC^6 + 0.2484SOC^5 - 0.3462SOC^4 + 0.2572SOC^3 - 0.0890SOC^2 + 0.0134SOC + 0.001$
		C_0	F	$C_0 = 969.2571SOC^6 + 887.6013SOC^5 + 1178.589SOC^4 + 884.2022SOC^3 + 1021.6423SOC^2 + 982.9249SOC + 949.3935$
		C_1	F	$C_1 = 66046.5149SOC^6 + 116235.5609SOC^5 - 716404.1789SOC^4 + 852777.47SOC^3 - 392608.1322SOC^2 + 74731.2758SOC + 4079.2979$
Second Order	(4) DP (Improved Thevenin) [19,22]	R_0	Ω	$R_0 = 0.0034SOC^6 + 0.0005SOC^5 - 0.0028SOC^4 - 0.0012SOC^3 + 0.0027SOC^2 + 0.0001SOC + 0.0001$
		R_1	Ω	$R_1 = -0.0663SOC^6 + 0.2344SOC^5 - 0.3503SOC^4 + 0.2661SOC^3 - 0.0852SOC^2 + 0.0132SOC + 0.0011$
		R_2	C_1	$R_2 = -0.0222SOC^6 + 0.0759SOC^5 - 0.1069SOC^4 + 0.0757SOC^3 - 0.0252SOC^2 + 0.0036SOC + 0.0002$
		C_1	F	$C_1 = 64059.2267SOC^6 + 114477.939SOC^5 - 655134.1246SOC^4 + 1156256.7687SOC^3 - 76280.5371SOC^2 + 179705.2612SOC + 5370.0249$
		C_2	F	$C_2 = -66069999.7769SOC^6 + 200004778.4783SOC^5 - 2.32301906.4313SOC^4 + 1.38646387.5308SOC^3 - 36166028.5118SOC^2 + 7398658.6212SOC + 83332.5804$
	(5) GNL (Improved DP) [23]	R_0	Ω	$R_0 = 0.0032SOC^6 - 0.0032SOC^5 + 0.0031SOC^4 - 0.0014SOC^3 + 0.001SOC^2 - 0.0001SOC$
		R_1	Ω	$R_1 = -0.0662SOC\text{^}6 + 0.2313SOC^5 - 0.3527SOC^4 + 0.2624SOC^3 - 0.0861SOC^2 + 0.0131SOC + 0.001$
		R_2	C_1	$R_2 = -0.0222SOC^6 + 0.076SOC^5 - 0.1057SOC^4 + 0.0745SOC^3 - 0.0252SOC^2 + 0.0036SOC + 0.0002$
		C_0	F	$C_0 = 995.5311SOC^6 + 989.7628SOC^5 + 978.2611SOC^4 + 954.1399SOC^3 + 900.7134SOC^2 + 776.5904SOC + 440.0053$
		C_1	F	$C_1 = 57078.7367SOC^6 + 107555.1108SOC^5 - 756122.6816SOC^4 + 889639.2846SOC^3 - 394186.2653SOC^2 + 93674.7316SOC + 4200.5308$
		C_2	F	$C_2 = -67383652.5763SOC^6 + 200030799.464SOC^5 - 233156409.4362SOC^4 + 135167762.9895SOC^3 - 40356464.4329SOC^2 + 6880723.553SOC + 80743.0041$
(6) Improved RC [19,20,24]		R_0	Ω	$R_0 = 0.0034SOC\text{^}6 - 0.0014SOC^5 + 0.0042SOC^4 - 0.0029SOC^3 + 0.0007SOC^2 + 0.0001$
		R_1	Ω	$R_1 = -0.0677SOC^6 + 0.2359SOC^5 - 0.342SOC^4 + 0.2609SOC^3 - 0.0908SOC^2 + 0.0164SOC + 0.0012$
		R_2	C_1	$R_2 = -0.0215SOC^6 + 0.0754SOC^5 - 0.1052SOC^4 + 0.0786SOC^3 - 0.0241SOC^2 + 0.0037SOC + 0.0005$
		C_1	F	$C_1 = 336133.6554SOC^6 - 173161.7203SOC^5 + 56453.1902SOC^4 + 664439.2213SOC^3 - 187981.7236SOC^2 + 34324.8044SOC - 976.6841$
		C_2	F	$C_2 = -66039255.7773SOC^6 + 199336970.6359SOC^5 - 233768933.8113SOC^4 + 134938550.9402SOC^3 - 42125510.64SOC^2 + 6083989.9682SOC + 93971.9972$
(7) Shepherd [25,26]		K	Ω	-0.0003
		R_0	Ω	0.0015
(8) Unnewehr Universal [26]		K	Ω	0.0042
		R_0	Ω	0.0016
(9) Nernst [26]		K_0	Ω	-0.0004
		K_1	Ω	0.0013
		R_0	Ω	0.0016
(10) Fang (Improved Nernst) [27]		K_0	Ω	0.0056
		K_1	Ω	0.0173
		R_0	Ω	0.0017
		τ_1	No Unit	846.9308
		τ_2	No Unit	7.1227
(11) Liu [28]		t_c	s	193.56
		K	Ω	0
		A	V	-0.0017
		B	Ah^{-1}	-0.072
		R_0	Ω	0.0016

TABLE 3. *(Continued.)* **Optimized ECM parameter data.**

(12) Tremblay1 [29]	K	Ω	0.0028
	A	V	0
	B	Ah^{-1}	0.5251
	R_0	Ω	0.0012
(13) Tremblay2 [30,31]	t_c	s	1.5116
	K	Ω	-0.0018
	A	V	0
	B	Ah^{-1}	1.0249
	R_0	Ω	0.0027
(14) Plett [32- 9]	K_0	Ω	0.0022
	K_1	Ω	-0.0009
	K_2	Ω	0.0064
	K_3	Ω	0.0051
	K_4	Ω	-0.0002
	R_0	Ω	0.0016

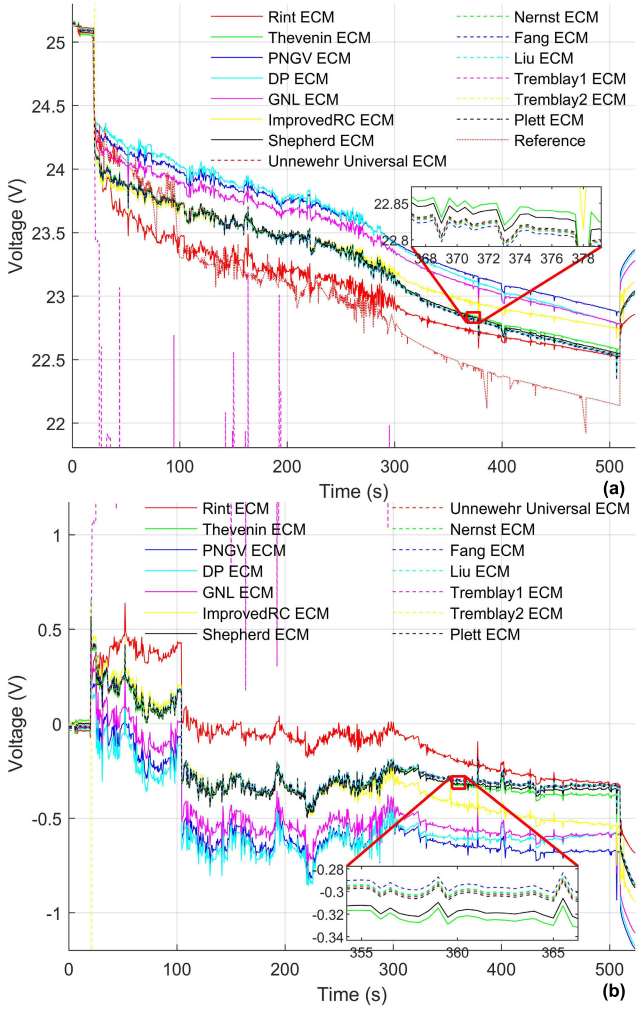

FIGURE 6. Battery pack voltage profiles of U_{cc} with 0 kg: (a) voltage profile, (b) fluctuation deviation.

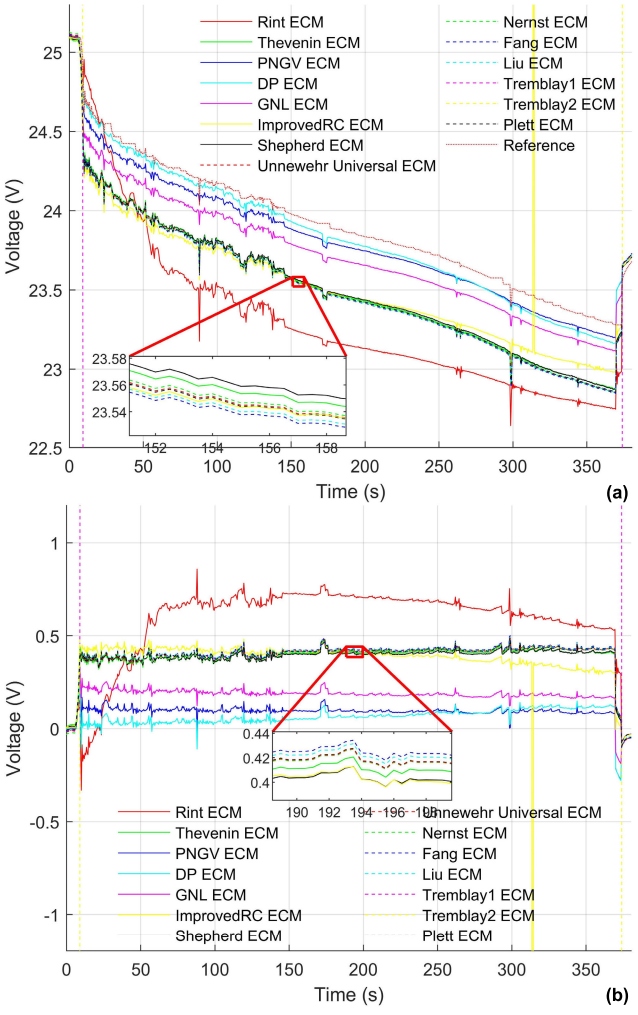

FIGURE 7. Battery pack voltage profiles of U_{cc} with 10 kg: (a) voltage profile, (b) fluctuation deviation.

worked best, resulting in the lowest RMS (0.0702 V) and maximum errors (0.6844 V).

3) In the case of the real flight test (colored blue), that is, U_{cc}, carrying a 10 kg payload, (7) the Shepherd ECM worked best, resulting in the lowest RMS (0.0875 V) and SD errors (0.0872 V).

By analyzing the above phenomena, we derived the generally applicable characteristics of the 14 ECMs, as described below.

TABLE 4. Error analysis.

ECM Type		Error (V) (1st Row: Mean, 2nd Row: RMS, 3rd Row: SD, 4th Row: Max)		
		U_{oc}	U_{cc} (w/ 0 kg)	U_{cc} (w/ 10 kg)
First Order	(1) Rint [19-21]	-0.0004	-0.0004	-0.0168
		0.058	0.0702	0.1221
		0.058	0.0702	0.1210
		0.6699	0.6844	0.8588
	(2) Thevenin [22]	0.0045	0.0149	-0.0024
		0.0380	0.0768	0.0897
		0.0377	0.0754	0.0896
		0.7575	0.8631	0.8631
	(3) PNGV (Improved Thevenin) [19,20]	0.0264	0.0465	0.0298
		0.0773	0.1411	0.1085
		0.0726	0.1333	0.1044
		0.6532	1.1917	1.1917
Second Order	(4) DP (Improved Thevenin) [19,22]	0.0231	0.0425	0.0261
		0.0751	0.1371	0.1007
		0.0715	0.1303	0.0973
		0.6718	1.1751	1.1751
	(5) GNL (Improved DP) [23]	0.019	0.0365	0.0196
		0.0612	0.1203	0.0961
		0.0582	0.1146	0.0941
		0.7088	1.1064	1.1064
(6) Improved RC [19,20,24]		0.0291	0.0412	0.0242
		0.077	0.1106	0.1288
		0.0713	0.1027	0.1265
		0.9777	0.9777	8.6475
(7) Shepherd [25,26]		0.0007	0.0108	-0.0064
		0.0371	0.0753	0.0875
		0.0371	0.0745	0.0872
		0.6372	0.8685	0.8685
(8) Unnewehr Universal [26]		0.0139	0.0226	0.0053
		0.0414	0.0754	0.0902
		0.039	0.0719	0.09
		0.8018	0.85	0.85
(9) Nernst [26]		0.0117	0.02	0.0027
		0.0413	0.0749	0.0896
		0.0396	0.0721	0.0895
		0.8158	0.8475	0.8475
(10) Fang (Improved Nernst) [27]		0.0156	0.0242	0.0069
		0.0419	0.0749	0.0911
		0.0388	0.0709	0.0908
		0.8079	0.8449	0.8449
(11) Liu [28]		0.0153	0.0244	0.0072
		0.0376	0.0733	0.0892
		0.0343	0.0692	0.0889
		0.6159	0.8528	0.8528
(12) Tremblay1 [29]		0.0156	-0.7261	-1.2543
		0.0418	18.4553	36.4302
		0.0388	18.4414	36.4093
		0.8135	2877.5274	2891.3378
(13) Tremblay2 [30,31]		0.004	5129.9020	19788.6205
		0.0397	770508.7184	1549746.3695
		0.0395	770506.7405	1549650.3923
		0.8134	123075097.9830	124151968.0769
(14) Plett [32- 9]		0.0156	0.0247	0.0074
		0.0377	0.0737	0.0889
		0.0344	0.0695	0.0866
		0.6472	0.8536	0.8536

1) Heavier ECMs containing more arguments (representatively, (11) Liu ECM) resulted in a smaller error, but had weaker adaptability to the dynamic discharging loads, resulting in a larger error.
2) Lighter ECMs containing fewer arguments (representatively, (1) Rint ECM) resulted in a larger error but had great adaptability to the dynamic discharging loads, resulting in a smaller error.
3) ECMs containing varying parameters with sixth-degree polynomials depending on the SOC ((1) Rint, (2) Thevenin, (3) PNGV, (4) DP, (5) GNL, and (6) Improved RC ECMs) resulted in worse error values, longer data fitting times, and difficulties in real-life implementation because of the use of more memory in the BMS chip.
4) We chose the (7) Shepherd ECM as the best candidate ECM for real-life applications because it has the simplest formula with only two constant parameters.

Each of the 14 ECMs listed in this manuscript consists of different mathematical formats having different parameter sets and this results in different reactance behavior which brings differences for mean, SD, RMS, and max error values. The main purpose of this manuscript is to analyze the different error dynamics upon a real flight current pattern.

IV. CONCLUSION

In this manuscript, we summarized a total of 14 well-known ECMs by presenting a schematic diagram and the corresponding equations which are implemented in the MATLAB/Simulink environment. We first extracted ECM parameters through the HPPC tests based on the curve-fitting method. Then, we applied real flight current patterns to evaluate the error characteristics of 14 ECMs based on error fluctuation deviation analysis. In particular, we focused on evaluating the ECM in terms of accuracy (mean, RMS, SD, and maximum values).

In summary, the Liu ECM resulted in the lowest RMS (0.0376 V), SD (0.0343 V), and maximum errors (0.6159 V) for the HPPC test, the Rint ECM resulted in the lowest RMS (0.0702 V) and maximum errors (0.6844 V) for the real flight test carrying a 0 kg payload, and the Shepherd ECM resulted in the lowest RMS (0.0875 V) and SD errors (0.0872 V) for the real flight test carrying a 10 kg payload.

Overall, we recommend the Shepherd ECM to obtain constant parameters owing to its fast parameter optimization convergence time and flexibility to dynamic discharging loads with a smaller error. The opposite phenomenon was observed in the ECMs with SOC-dependent parameters, resulting in longer data-fitting times and larger errors.

In the future, as a successive work, we will analyze well-known battery state estimation algorithms by combining them with ECMs listed in this manuscript to determine the fluctuation error characteristics.

REFERENCES

[1] B. Zhang, Z. Song, F. Zhao, and C. Liu, "Overview of propulsion systems for unmanned aerial vehicles," *Energies*, vol. 15, no. 455, pp. 1–25, Jan. 2022.
[2] ICAO. *Environmental Protection: Aircraft Engine Emissions*. Accessed: Jun. 17, 2023. [Online]. Available: http://www.icao.int/ environmental-protection/Pages/aircraft-engine-emissions.aspx

[3] J. E. Penner, D. H. Lister, D. J. Griggs, D. J. Dokken, and M. McFarland, "IPCC special report: Aviation and the global atmosphere," Intergovernmental Panel Climate Change, Geneva, Switzerland, Tech. Rep., 1999.
[4] D. J. Travis, A. M. Carleton, and R. G. Lauritsen, "Contrails reduce daily temperature range," *Nature*, vol. 418, no. 6898, pp. 601–602, Aug. 2002.
[5] G. P. Brasseur, M. Gupta, B. E. Anderson, S. Balasubramanian, S. Barrett, and D. Duda, "Impact of aviation on climate: FAA's aviation climate change research initiative (ACCRI) phase II," *Bull. Amer. Meteorolog. Soc.*, vol. 97, no. 4, pp. 561–583, Apr. 2016.
[6] T. Ryley, S. Baumeister, and L. Coulter, "Climate change influences on aviation: A literature review," *Transp. Policy*, vol. 92, pp. 55–64, Jun. 2020.
[7] R. D. Anderson, Y. Zhao, X. Wang, X. G. Yang, and Y. Li, "Real time battery power capability estimation," in *Proc. Amer. Control Conf. (ACC)*, Jun. 2012, pp. 592–597.
[8] S. Yuan, H. Wu, and C. Yin, "State of charge estimation using the extended Kalman filter for battery management systems based on the ARX battery model," *Energies*, vol. 6, no. 1, pp. 444–470, Jan. 2013.
[9] Z. He, M. Gao, C. Wang, L. Wang, and Y. Liu, "Adaptive state of charge estimation for Li-ion batteries based on an unscented Kalman filter with an enhanced battery model," *Energies*, vol. 6, no. 8, pp. 4134–4151, Aug. 2013.
[10] M. Gao, Y. Liu, and Z. He, "Battery state of charge online estimation based on particle filter," in *Proc. 4th Int. Congr. Image Signal Process.*, vol. 4, Oct. 2011, pp. 2233–2236.
[11] S. Park, J. Ahn, T. Kang, S. Park, Y. Kim, I. Cho, and J. Kim, "Review of state-of-the-art battery state estimation technologies for battery management systems of stationary energy storage systems," *J. Power Electron.*, vol. 20, pp. 1526–1540, Aug. 2020.
[12] X. Hu, F. Feng, K. Liu, L. Zhang, J. Xie, and B. Liu, "State estimation for advanced battery management: Key challenges and future trends," *Renew. Sustain. Energy Rev.*, vol. 114, Oct. 2019, Art. no. 109334.
[13] A. Hobbs and S. R. Herwitz, "Human challenges in the maintenance of unmanned aircraft systems," FAA and NASA Interim, Washington, DC, USA, Tech. Rep., May 2006.
[14] B. Saha, E. Koshimoto, C. C. Quach, E. F. Hogge, T. H. Strom, B. L. Hill, S. L. Vazquez, and K. Goebel, "Battery health management system for electric UAVs," in *Proc. Aerosp. Conf.*, Mar. 2011, pp. 1–9.
[15] B. Bole, M. Daigle, and G. Gorospe, "Online prediction of battery discharge and estimation of parasitic loads for an electric aircraft," in *Proc. Eur. Conf. Prognostics Health Manage. Soc.*, Jul. 2014, pp. 1–10.
[16] Y. Tian, C. Chen, B. Xia, W. Sun, Z. Xu, and W. Zheng, "An adaptive gain nonlinear observer for state of charge estimation of lithium-ion batteries in electric vehicles," *Energies*, vol. 7, no. 9, pp. 5995–6012, Sep. 2014.
[17] Z. Guo, X. Qiu, G. Hou, B. Y. Liaw, and C. Zhang, "State of health estimation for lithium ion batteries based on charging curves," *J. Power Sources*, vol. 249, pp. 457–462, Mar. 2014.
[18] G. L. Plett, "High-performance battery-pack power estimation using a dynamic cell model," *IEEE Trans. Veh. Technol.*, vol. 53, no. 5, pp. 1586–1593, Sep. 2004.
[19] H. He, R. Xiong, and J. Fan, "Evaluation of lithium-ion battery equivalent circuit models for state of charge estimation by an experimental approach," *Energies*, vol. 4, no. 4, pp. 582–598, Mar. 2011.
[20] V. H. Johnson, "Battery performance models in ADVISOR," *J. Power Sources*, vol. 110, no. 2, pp. 321–329, Aug. 2002.
[21] S. Nejad, D. T. Gladwin, and D. A. Stone, "A systematic review of lumped-parameter equivalent circuit models for real-time estimation of lithium-ion battery states," *J. Power Sources*, vol. 316, pp. 183–196, Jun. 2016.
[22] H. He, R. Xiong, X. Zhang, F. Sun, and J. Fan, "State-of-charge estimation of the lithium-ion battery using an adaptive extended Kalman filter based on an improved Thevenin model," *IEEE Trans. Veh. Technol.*, vol. 60, no. 4, pp. 1461–1469, May 2011.
[23] M. Shen and Q. Gao, "A review on battery management system from the modeling efforts to its multiapplication and integration," *Int. J. Energy Res.*, vol. 43, no. 10, pp. 5042–5075, Aug. 2019.
[24] V. H. Johnson, A. A. Pesaran, and T. Sack, "Temperature-dependent battery models for high-power lithium-ion batteries," in *Proc. Annu. Electr. Vehicle Symp.*, Jan. 2001, pp. 1–14.
[25] C. M. Shepherd, "Design of primary and secondary cells: II. An equation describing battery discharge," *J. Electrochem. Soc.*, vol. 112, no. 7, pp. 657–664, 1965.
[26] J. Meng, G. Luo, M. Ricco, M. Swierczynski, D. Stroe, and R. Teodorescu, "Overview of lithium-ion battery modeling methods for state-of-charge estimation in electrical vehicles," *Appl. Sci.*, vol. 8, no. 659, pp. 1–17, Apr. 2018.
[27] H. Fang, X. Zhao, Y. Wang, Z. Sahinoglu, T. Wada, S. Hara, and R. A. de Callafon, "State-of-charge estimation for batteries: A multi-model approach," in *Proc. Amer. Control Conf.*, Jun. 2014, pp. 2779–2785.
[28] L. Liu, L. Y. Wang, Z. Chen, C. Wang, F. Lin, and H. Wang, "Integrated system identification and state-of-charge estimation of battery systems," *IEEE Trans. Energy Convers.*, vol. 28, no. 1, pp. 12–23, Mar. 2013.
[29] O. Tremblay, L.-A. Dessaint, and A.-I. Dekkiche, "A generic battery model for the dynamic simulation of hybrid electric vehicles," in *Proc. IEEE Vehicle Power Propuls. Conf.*, Sep. 2007, pp. 284–289.
[30] O. Tremblay and L.-A. Dessaint, "Experimental validation of a battery dynamic model for EV applications," *World Electr. Vehicle J.*, vol. 3, no. 2, pp. 289–298, Jun. 2009.
[31] The Mathworks, Inc. *Battery: Generic Battery Model*. Accessed: Jun. 17, 2023. [Online]. Available: http://www.mathworks.co.kr/kr/help/physmod/sps/powersys/ref/battery.html
[32] G. L. Plett, "Extended Kalman filtering for battery management systems of LiPB-based HEV battery packs: Part 2. Modeling and identification," *J. Power Sources*, vol. 134, no. 2, pp. 262–276, 2004.
[33] A. Seaman, T.-S. Dao, and J. McPhee, "A survey of mathematics-based equivalent-circuit and electrochemical battery models for hybrid and electric vehicle simulation," *J. Power Sources*, vol. 256, pp. 410–423, Jun. 2014.

SUNGHUN JUNG (Member, IEEE) received the B.S. degree in mechanical engineering from the University of Minnesota, Twin Cities, USA, in 2009, and the M.S. and Ph.D. degrees in mechanical engineering from Purdue University, West Lafayette, USA, in 2010 and 2013, respectively.

He was a Principal Researcher with Samsung SDI, from 2014 to 2016. He has been an Assistant Professor with the Faculty of Smart Vehicle System Engineering, Chosun University. His current research interests include control and optimization for autonomous operations of unmanned assets, particularly UAVs.

ABERA TULLU (Member, IEEE) received the B.Sc. degree in applied physics and the M.Sc. degree in astrophysics from Addis Ababa University, Ethiopia, in 2003 and 2007, respectively, and the Ph.D. degree in aerospace engineering from Pusan National University, South Korea, in 2017. He was a Postdoctoral Researcher with the Aerospace Engineering Department, Pusan National University, from March 2017 to February 2020. He was an Assistant Professor of aerospace engineering with Sejong University, South Korea, from March 2020 to February 2023. He is currently a Research Associate with Korea Aerospace University, South Korea. His current research interests include unmanned aerial vehicle-based target tracking, path planning, obstacle avoidance, and aerial robot arm design and control.